Available online at www.sciencedirect.com
SCIENCE DIRECT®
ELSEVIER
Earth and Planetary Science Letters 217 (2003) 111–122
EPSL
www.elsevier.com/locate/epsl

Slowing extrusion tectonics: lowered estimate of post-Early Miocene slip rate for the Altyn Tagh fault

Yongjun Yue [a,*], Bradley D. Ritts [b], Stephan A. Graham [a], Joseph L. Wooden [c], George E. Gehrels [d], Zhicheng Zhang [e]

[a] *Department of Geological and Environmental Sciences, Stanford University, Stanford, CA 94305-2115, USA*
[b] *Department of Geology, Utah State University, Logan, UT 84322-4505, USA*
[c] *U.S. Geological Survey, 345 Middlefield Road, Menlo Park, CA 90425, USA*
[d] *Department of Geosciences, University of Arizona, Tucson, AZ 85721-0077, USA*
[e] *Department of Geology, Peking University, Beijing 100871, PR China*

Received 18 March 2003; received in revised form 19 August 2003; accepted 19 September 2003

Abstract

Determination of long-term slip rate for the Altyn Tagh fault is essential for testing whether Asian tectonics is dominated by lateral extrusion or distributed crustal shortening. Previous slip-history studies focused on either Quaternary slip-rate measurements or pre-Early Miocene total-offset estimates and do not allow a clear distinction between rates based on the two. The magmatic and metamorphic history revealed by SHRIMP zircon dating of clasts from Miocene conglomerate in the Xorkol basin north of the Altyn Tagh fault strikingly matches that of basement in the southern Qilian Shan and northern Qaidam regions south of the fault. This match requires that the post-Early Miocene long-term slip rate along the Altyn Tagh fault cannot exceed 10 mm/year, supporting the hypothesis of distributed crustal thickening for post-Early Miocene times. This low long-term slip rate and recently documented large pre-Early Miocene cumulative offset across the fault support a two-stage evolution, wherein Asian tectonics was dominated by lateral extrusion before the end of Early Miocene, and since then has been dominated by distributed crustal thickening and rapid plateau uplift.

Keywords: Altyn Tagh fault; post-Early Miocene slip rate; Xorkol basin; provenance analysis; SHRIMP zircon dating

1. Introduction

The India–Eurasia collision is one of the most prominent geological events of the past 100 Myr. Determination of how more than 2000 km of convergence between these two continents [1] was accommodated has profound implications for understanding the mechanics of continental deformation. Two contrasting end-member mechanisms have been developed over the past few decades. The lateral extrusion hypothesis emphasizes the existence of a few large strike-slip faults and argues that these faults allow lateral extrusion to accommodate a majority of the convergence [2,3]. This hypothesis implies large cumulative off-

* Corresponding author. Tel.: +1-650-724-2627; Fax: +1-650-725-0979.
E-mail address: yongjun@pangea.stanford.edu (Y. Yue).

0012-821X/03/$ – see front matter © 2003 Elsevier B.V. All rights reserved.
doi:10.1016/S0012-821X(03)00544-2

sets and fast slip rates (>10 mm/year) on the strike-slip faults. In contrast, the distributed crustal thickening hypothesis emphasizes the existence of widespread thrust faults and low viscosity of Tibetan lithosphere, and suggests that shortening of both crust and lithospheric mantle has been much more important than lateral extrusion. This hypothesis predicts small cumulative offsets and low slip rates on the strike-slip faults emphasized in the extrusion model [4–6].

Although no other feature in Tibet is a better candidate for testing these two hypotheses than the Altyn Tagh fault (ATF), a 1600-km-long active left-slip fault defining the northern edge of the Tibet Plateau (Fig. 1), recent studies have produced conflicting interpretations of its slip history. Global positioning system measurements (9±5 mm/year) [7,8] and some low-bound Quaternary slip-rate estimates (2–6 mm/year [9]; ~10 mm/year [10]) suggest low slip rates for the fault, supporting the distributed thickening hypothesis. On the other hand, various pre-Early Miocene piercing points demonstrate that the fault has a cumulative Cenozoic offset of 375±25 km along its eastern and central strands [11–18], and some high-bound Quaternary slip-rate estimates suggest that the fault has a slip rate of 20–30 mm/year [19–22], supporting the lateral extrusion hypothesis. Previous understanding of the long-term slip rate along the ATF (14±2 mm/year) has not been sufficiently detailed to evaluate these two conflicting views because of the paucity of Miocene piercing points (dashed line in Fig. 2) [17].

In this communication, we report our provenance analysis of the upper Lower Miocene and the overlying younger Miocene strata of the Xorkol basin (Fig. 1), which places a key constraint on the long-term slip rate along the ATF and extends the low present and Quaternary slip-rate estimates back to the middle Miocene. Our data and interpretations support a two-stage model [23], which, as a reconciliation between the previous two end-member hypotheses, proposes an Oligocene–Early Miocene phase of rapid extrusion and a post-Early Miocene crustal thickening phase associated with reduced slip rate along the ATF.

2. Geology of the Xorkol basin

2.1. Basement geology

The Xorkol basin is an east–west Tertiary basin bounded on its southeastern side by the ATF (Fig. 3). The northern and southern boundaries of the basin are high-angle to nearly vertical reverse faults, with upthrown basement. The north-

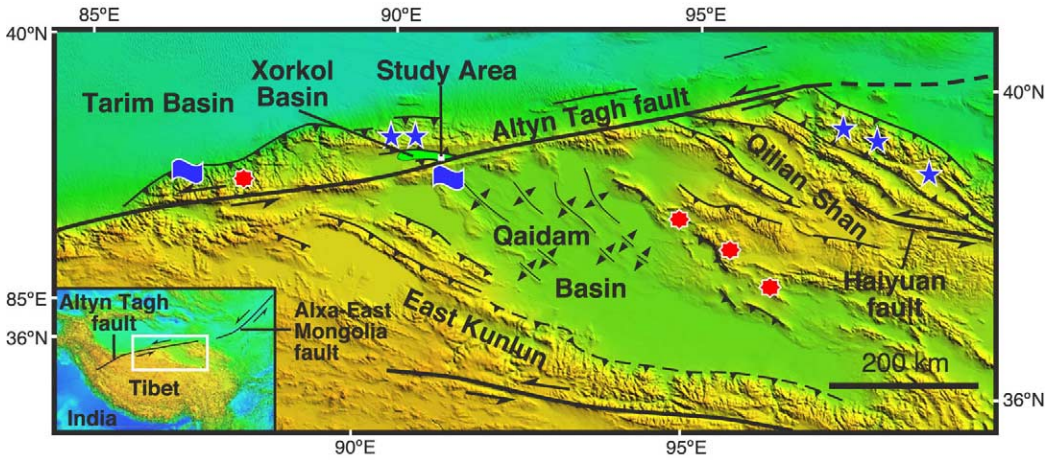

Fig. 1. Topographic map showing locations of ATF, Xorkol basin study area, and previously documented piercing points [17]. Barbed line: thrust fault; line with opposing triangles: anticline; blue star: blueschist locality; red polygon: eclogite locality; blue flag: Jurassic shoreline.

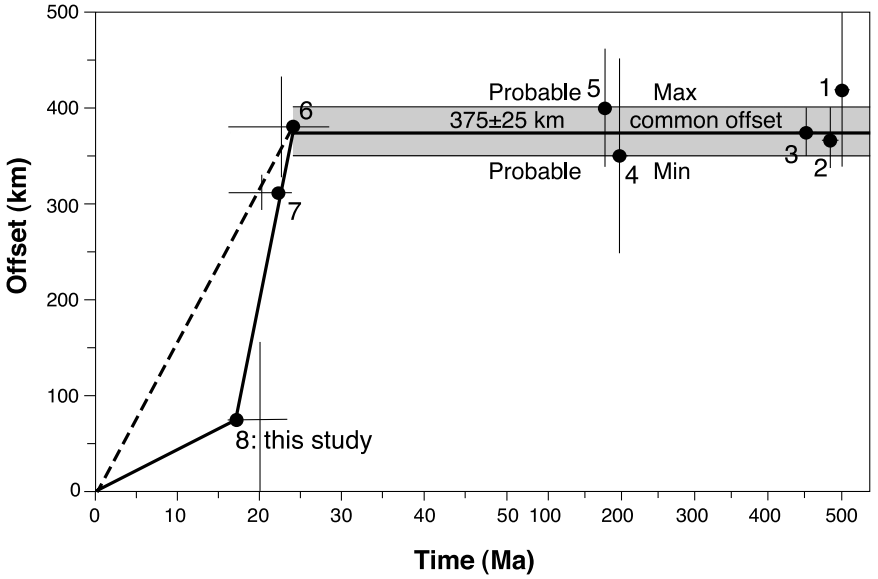

Fig. 2. Time–displacement graph for the ATF, as originally proposed by Yue et al. [17] using offset markers shown in Fig. 1 (dashed line), and higher-resolution time–displacement curve incorporating new detrital-zircon data presented in this paper (solid line). The curve does not include estimates of Wang [41] and Yin et al. [42], which have been previously argued as mis-matches by Yue et al. [17] and Ritts et al. [29]. A new piercing point (point 2) by Gehrels et al. [18] is added. Piercing points: 1, southern Altyn Tagh–northern Qaidam eclogite correlation [16]; 2, northern Qilian–northern Altyn Tagh 490–480-Myr-old magmatic arc correlation [18]; 3, northern Qilian–northern Altyn Tagh suture correlation [11,14,15], 4, Jurassic cooling zone correlation [13], 5, Jurassic shoreline correlation [12]. Piercing points 6 and 7 are derived from our previous clast-source terrane correlation [17] and piercing point 8 is obtained from the current study. Although age uncertainties are indicated by error bars, our preferred age interpretations for piercing points 6 and 8 (shown by filled black circles) are Oligocene/Miocene boundary and latest Early Miocene because our cross-fault matches come from the uppermost Oligocene–lowest Miocene strata and the top part of the Lower Miocene strata, respectively. The age of piercing point 7 must be between those of piercing points 6 and 8 because of its stratigraphic position. The probable offset of piercing point 8 is 82.5 km, which is the median value of the current error range.

ern fault boundary dips to the north 45–60°, and the southern fault boundary dips to the south 65–85° [24].

The basement to the north of the basin includes Archean to Paleoproterozoic strata and Mesoproterozoic–lower Paleozoic undifferentiated subduction complex and convergent-margin sequences. The Archean–Paleoproterozoic basement rocks include gneiss, granulite, plagioclase, amphibolite and migmatite. These rocks are thrust over the Mesoproterozoic–lower Paleozoic undifferentiated subduction complex and convergent-margin rocks [11]. The subduction complex is characterized by ophiolite and high-pressure metamorphic rocks [25], and is considered to be the offset equivalent of the North Qilian subduction complex [11,14,15]. The convergent-margin sequence consists of andesite, dacite, rhyolite, turbidites, chert and carbonate. These assemblages are intruded by Paleoproterozoic and early Paleozoic granitoids.

The basement to the south of the basin is composed mainly of a slightly metamorphosed Mesoproterozoic passive-margin sequence, including slate, phyllite, and slightly metamorphosed sandstone, carbonate and chert. Both our field study and previous geological mapping indicate that neither granitic intrusives nor high-grade metamorphic rocks occur to the south of the basin [24,26].

The basement to the east of the basin is located on the southern side of the ATF, and is mainly composed of Paleoproterozoic Dakendaban Group, and early and late Paleozoic and Mesozoic granite intrusives [11,26,27].

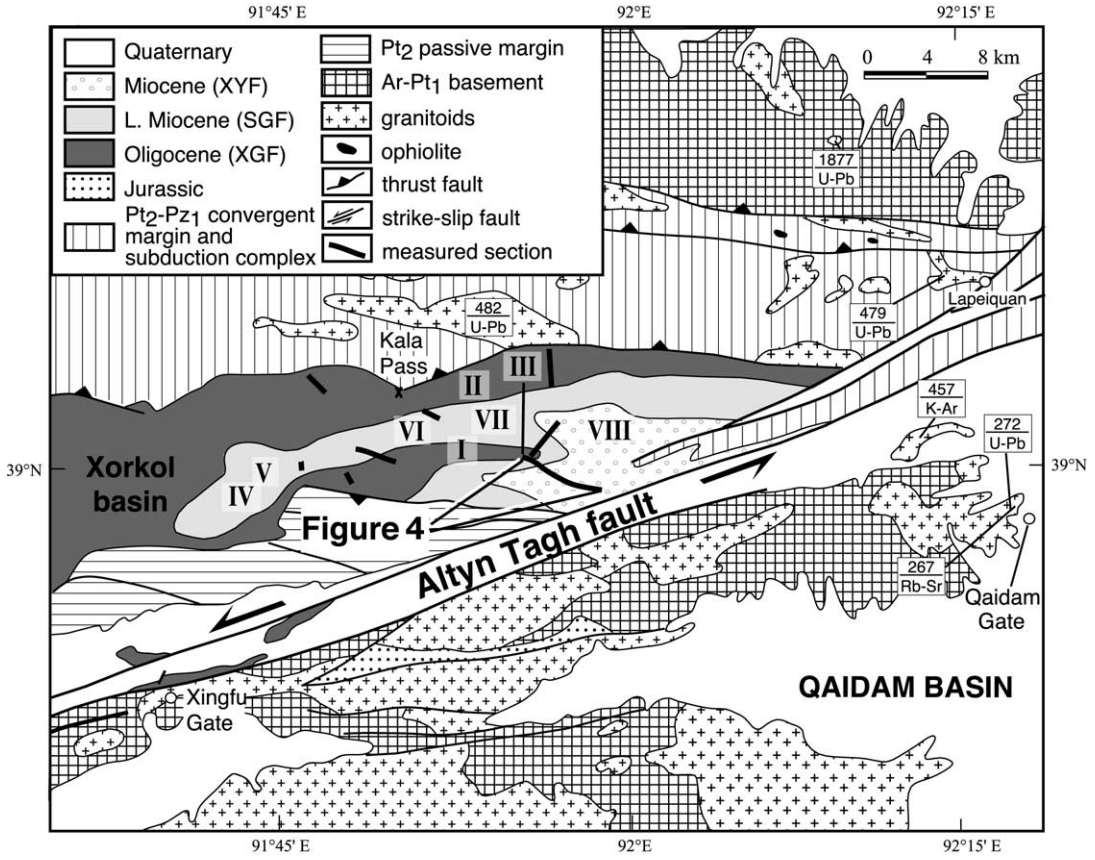

Fig. 3. A simplified geologic map of the Xorkol basin (after [11,26,33]). Symbols I to VIII indicate locality of fossils; numbers represent age dating results (in Ma) and U–Pb, Rb–Sr and K–Ar below the numbers indicate radiometric dating methods. XGF, Xiaganchaigou Formation; SGF, Shangganchaigou Formation; XYF, Xiayoushashan Formation.

2.2. Age constraints on Tertiary basin fill

The basin fill in the Xorkol basin includes the Oligocene Xiaganchaigou Formation, the Lower Miocene Shangganchaigou Formation, and the Miocene Xiayoushashan Formation. As shown in Table 1 and Fig. 3, all of these formations contain fossils, which form the basis for age determinations.

Table 1
Tertiary fossils of the Xorkol basin

Locality	Fossil
I (Xiaganchaigou Fm.)	*Sphaerium* cf. *rivicolum*
II (Xiaganchaigou Fm.)	*Ilyocypris* cf. *errabundis*
III (Xiaganchaigou Fm.)	*Ilyocypris errabundis*, *Candoniella marcida*, *Eurypris* sp.
IV (Shangganchaigou Fm.)	*Radix* sp., *Planorbis* sp., *Pupilla* sp., *Galba* sp., *Gyraulus* sp., *Neritodonta* sp., *Candoniella marcida*
V (Shangganchaigou Fm.)	*Planorbis* sp., *Pupilla* sp.
VI (Shangganchaigou Fm.)	*Radix* sp., *Planorbis* sp.
VII (Shangganchaigou Fm.)	*Radix* sp.
VIII (Xiayoushashan Fm.)	*Radix* sp., *Planorbis* sp.

Locality is shown in Fig. 3 and data source is [26].

The Oligocene age of the Xiaganchaigou Formation is based on the occurrence of a fossil assemblage, including ostracods (*Ilyocypris errabundis*, *Candoniella marcida*, *Eurypris* sp.) and bivalve (*Sphaerium* cf. *rivicolum*) (Table 1). Among these fossils, *Ilyocypris errabundis* is an important species in Oligocene strata in the adjacent Qaidam basin, the Junggar basin and the North China basin; *Candoniella marcida* occurs mainly in Oligocene–Lower Miocene strata in the Qaidam basin [26–28].

The Lower Miocene Shangganchaigou Formation contains an Early Miocene fossil assemblage consisting of gastropods (*Radix* sp., *Planorbis* sp., *Pupilla* sp., *Galba* sp., *Gyraulus* sp., *Neritodonta* sp.) and ostracods (*Candoniella marcida*) (Table 1). This fossil assemblage is characterized by the absence of *Ilyocypris errabundis* and its abundant

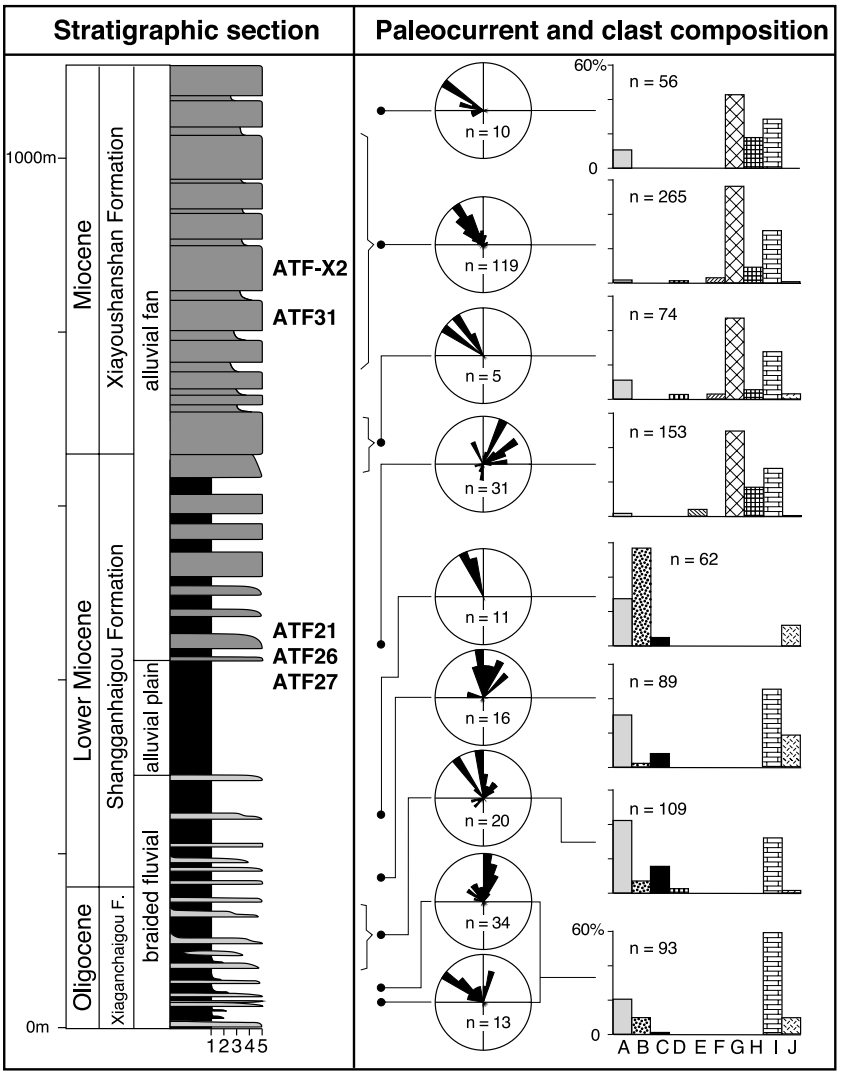

Fig. 4. Detailed stratigraphic section, paleocurrent measurements, and clast compositions of the eastern Xorkol basin. 1, mudstone; 2, very fine sandstone; 3, sandstone; 4, very coarse sandstone; and 5, conglomerate. Conglomerate clast lithology: A, slate and phyllite; B, sandstone; C, volcanic rock; D, chert; E, schist; F, quartzite; G, gneiss; H, granite; I, carbonate; J, vein quartz; n = number of measurements.

gastropod fossils, such as *Radix* sp., *Planorbis* sp., *Pupilla* sp. In the Qaidam basin, these gastropod fossils occur mainly in Miocene and younger strata. This fact and the occurrence of *Candoniella marcida*, which mainly occurs in Oligocene–Lower Miocene strata in the Qaidam basin, suggest an Early Miocene age for the formation [26].

The fossil assemblage in the Xiayoushashan Formation (Table 1) constrains the age as Neogene. The Miocene age of the Xiayoushashan Formation is based on this assemblage and its apparently conformable contact with the better-dated, underlying Shangganchaigou Formation [26].

3. Provenance analysis

3.1. Depositional environments, paleocurrent analysis and clast composition

We conducted a provenance study of Oligocene and Miocene strata in the eastern part of the Xorkol basin adjacent to the ATF from 1998 to 2002, including measurement of eight stratigraphic sections, collection of paleocurrent data and modal analysis of conglomerate clast composition [24].

As shown in Fig. 4, the Oligocene Xiaganchaigou Formation and the lower member of the Lower Miocene Shangganchaigou Formation are composed of pebble–cobble conglomerate units 2–8 m thick that are interbedded with massive reddish mudstone units up to a few meters thick. The conglomerate units are composed of well sorted and well organized amalgamated beds with sharp to erosive bases that are 1–2 m thick. Individual beds are commonly lenticular, although the amalgamated conglomerate bodies are laterally extensive. The interbedded mudstone units are red, massive and occasionally nodular. The coarse sediment caliber, imbrication, and good organization suggest that the sediment was transported in an energetic, unidirectional, subaqueous flow, which we interpret as braided fluvial channel flow. The mudstones are interpreted as overbank and playa deposits. Conglomerate clast types include limestone, sandstone, basalt, andesite, dacite, chert, slate, and vein quartz. Clast imbrication indicates north- to northwest-directed paleoflow, suggesting a source terrane to the southeast, now displaced by left-lateral slip on the ATF [17,24,29].

The middle unit, represented by the middle member of the Lower Miocene Shangganchaigou Formation, is an interval of red mudstone with local nodular carbonate horizons, thin interbedded sandstone beds and rare mudcracks deposited in alluvial-plain/playa environments [24,29].

The upper unit, the focus of this paper, includes the upper member of the Lower Miocene Shangganchaigou Formation and the Miocene Xiayoushashan Formation. The former is composed of interbedded cobble and boulder conglomerate and mudstone and the latter consists of boulder and cobble conglomerate with minor very coarse-grained sandstone. The conglomerate beds range from well organized, well sorted, imbricated, clast-supported conglomerate (Fig. 5A) to massive, unsorted, matrix-supported conglomerate (Fig. 5B), interpreted as reflecting an alluvial-fan depositional environment [29]. Imbrication in the conglomerate beds yields paleo- current data indicative of flow to the north and northwest (Figs. 4 and 5A), suggesting sediment derivation from across the ATF, as in the underlying formations. Conglomerate clast types are gneiss (Fig. 5C), granite (Fig. 5B,D), limestone, and slate. Clast lithology and size (Fig. 5) indicate that the clasts are first-cycle sediments derived directly from a basement source terrane.

3.2. SHRIMP zircon dating of granitic clasts

Five granitic clast samples were collected from the upper unit for sensitive high resolution ion microprobe (SHRIMP) zircon dating to characterize their source terranes (Figs. 3 and 4). Among these samples, ATF21, ATF26 and ATF27 were collected from the upper Lower Miocene Shangganchaigou Formation, and ATF31 and ATF-X2 were collected from the Miocene Xiayoushashan Formation.

As shown in Fig. 6 and Table 2, five zircon spot analyses from ATF21, a gneissic granite clast from the Shangganchaigou Formation, indicate

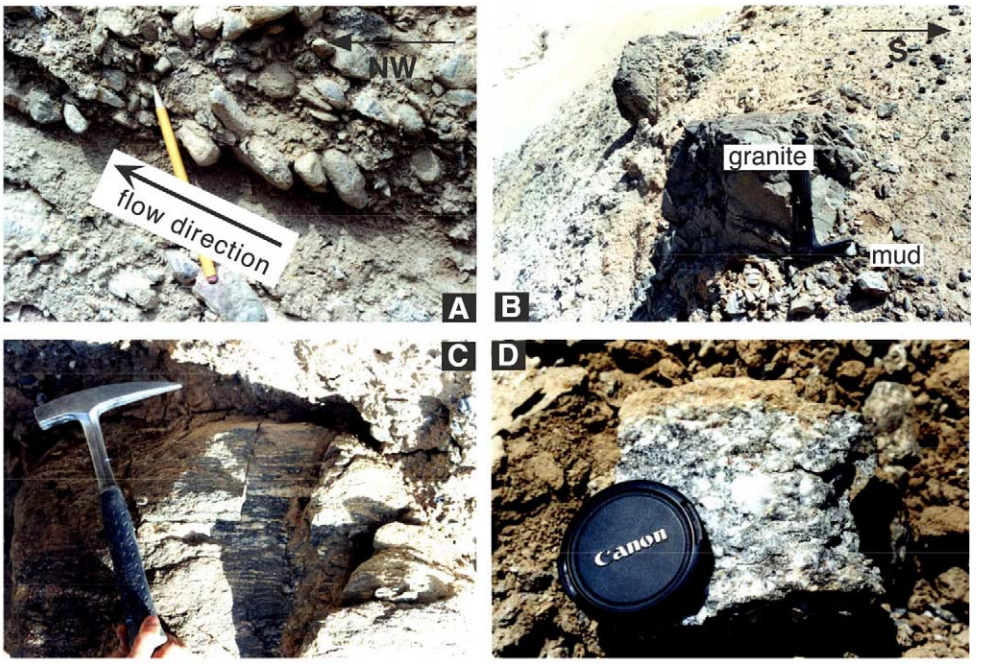

Fig. 5. Field photographs showing sedimentary structures and major clast types in the upper Lower Miocene–Miocene strata, Xorkol basin. (A) Well rounded, well imbricated and clast-supported cobble conglomerate. (B) Angular fine-grained granite boulder sitting in mud matrix. (C) A gneissic boulder. (D) A coarse-grained two-feldspar granite boulder.

that this rock crystallized between 459 Ma and 423 Ma, and one spot analysis on a grain edge suggests a metamorphic event at about 258 Ma. The low Th/U of this analysis is typical of zircon grown in a prograde metamorphic event (e.g. [30]). Six zircon ages from ATF26, a coarse-grained granodiorite clast, indicate that the rock crystallized at 262 ± 2 Ma, and four ages from ATF27, a monzogranite clast, indicate that the rock crystallized at approximately 249 ± 8 Ma.

Eleven zircon ages were obtained from sample ATF31, a foliated granodiorite clast from the Xiayoushashan Formation. These data indicate that the rock crystallized at 409 ± 7 Ma (six analyses) and two analyses with very low Th/U suggest metamorphism at 246 ± 3 Ma. Seven zircon ages from ATF-X2, a massive tonalite clast, indicate that the rock crystallized at 252 ± 3 Ma.

3.3. Sources of granite clasts

The SHRIMP zircon data illustrate that the source terrane(s) for the clasts in the upper Lower Miocene and the overlying Miocene formations underwent magmatic events in Silurian–earliest Devonian and Permian–earliest Triassic, and a metamorphic event in Permian–earliest Triassic. As shown in Fig. 7A, there is no appropriate source for the granitic clasts north of the ATF, consistent with paleocurrent results that indicate derivation of the clasts from the southern side of the fault.

Geological mapping [27,31] and radiometric dating [32,33] show a clear spatial segregation of granitic intrusives south of the ATF, in the Qilian Shan and Qaidam block. Granite bodies in northern and central Qilian Shan are Ordovician to Early Devonian in age (Fig. 7A) and lack Permian–earliest Triassic granitic plutons. However, both Silurian–earliest Devonian and Permian–earliest Triassic granitic bodies occur in southern Qilian Shan and northern Qaidam regions.

Fig. 7B presents crystallization ages recorded by the clasts in the Xorkol basin and single-zircon ages of the granitoids in the Qilian Shan and northern Qaidam [33]. It is clear from this corre-

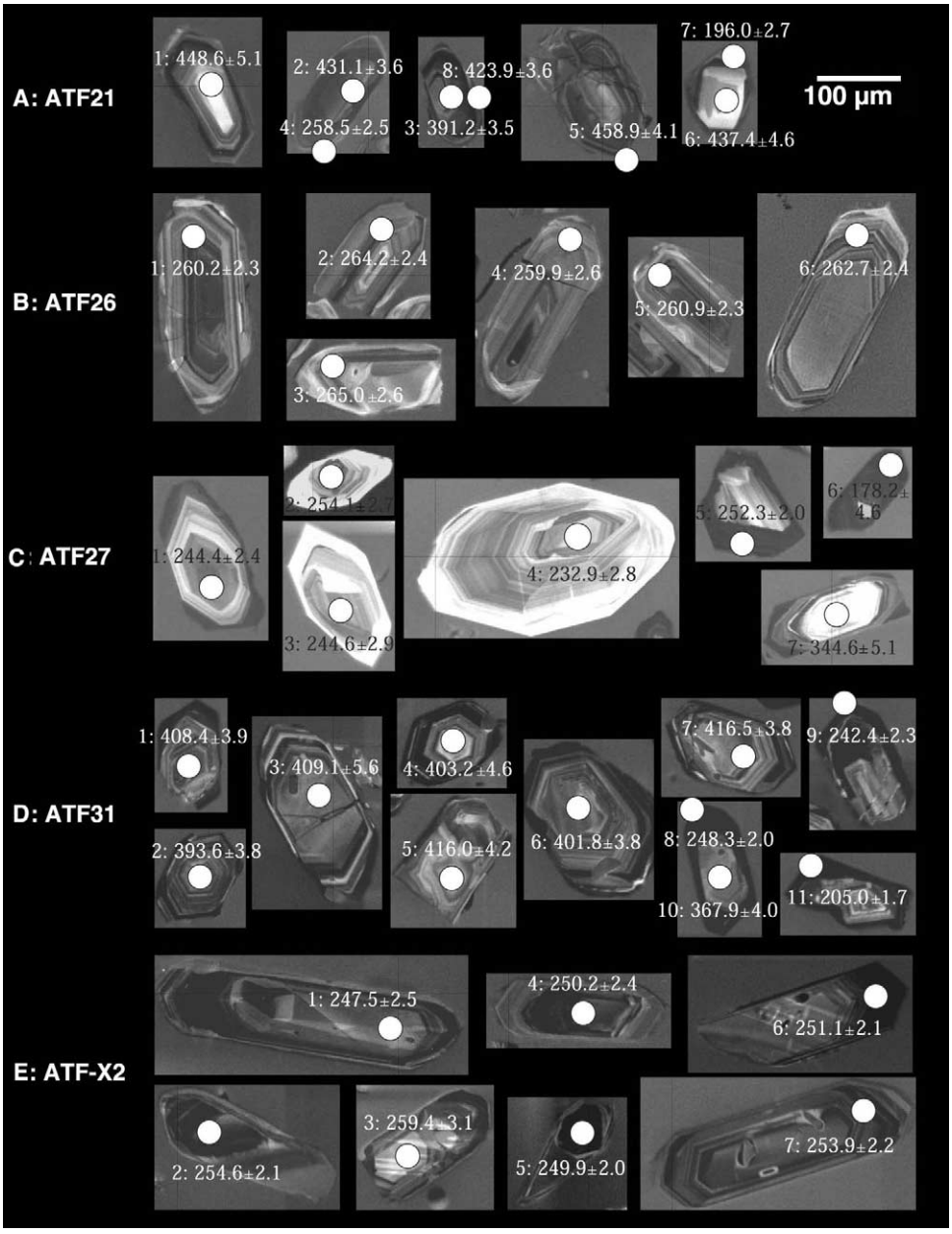

Fig. 6. Zircon images showing crystal structure and dating spots. Numbers indicate ^{207}Pb-corrected ^{206}Pb/^{238}U ages.

lation that only southern Qilian Shan and northern Qaidam can provide both Silurian–earliest Devonian and Permian–Triassic granitic clasts for the conglomerate units in the Xorkol basin. Petrologic study of a gneissic granite intrusive in the southern Qilian Shan demonstrates that the granite formed in the Silurian and then underwent a significant metamorphic event in the late Paleozoic [32], similar to the granite clasts of early Paleozoic age (Fig. 7C).

Table 2
SHRIMP zircon U–Pb dating results of Miocene clasts

Sample	U (ppm)	Th (ppm)	$^{232}Th/^{238}U$	^{207}Pb-corrected $^{206}Pb/^{238}U$ age (Ma)	±1σ (Ma)	Total $^{238}U/^{206}Pb$	±1σ (%)	Total $^{207}Pb/^{206}Pb$	±1σ (%)
ATF21-5	959	247	0.27	458.9	4.1	13.38	0.9	0.0663	1.2
ATF21-1	168	100	0.62	448.6	5.1	13.82	1.1	0.0593	2.5
ATF21-6	217	126	0.60	437.4	4.6	14.18	1.1	0.0594	2.2
ATF21-2	1240	714	0.60	431.1	3.6	14.24	0.8	0.0677	2.4
ATF21-8	1380	184	0.14	423.9	3.6	14.65	0.9	0.0586	2.0
ATF21-4	682	28	0.04	258.5	2.5	24.29	1.0	0.0566	1.9
ATF21-3	470	241	0.53	391.2[a]	3.5	15.81	0.9	0.0629	1.5
ATF21-7	951	70	0.08	196.0[a]	2.7	31.77	1.4	0.0654	3.5
ATF26-3	415	78	0.19	265.0	2.6	23.75	1.0	0.0542	2.1
ATF26-2	543	61	0.12	264.2	2.4	23.85	0.9	0.0534	1.8
ATF26-6	586	104	0.18	262.7	2.4	23.99	0.9	0.0531	1.8
ATF26-5	655	110	0.17	260.9	2.3	24.13	0.9	0.0540	1.7
ATF26-1	668	67	0.10	260.2	2.3	24.14	0.9	0.0560	1.6
ATF26-4	387	61	0.16	259.9	2.6	24.26	1.0	0.0527	2.3
ATF27-2	269	213	0.82	254.1	2.7	24.74	1.1	0.0557	2.6
ATF27-5	6818	1297	0.20	252.3	2.0	24.92	0.8	0.0557	0.7
ATF27-3	288	181	0.65	244.6	2.9	25.45	1.1	0.0637	6.5
ATF27-1	427	303	0.73	244.4	2.4	25.66	1.0	0.0578	2.1
ATF27-7	103	46	0.46	344.6[b]	5.1	17.89	1.5	0.0675	3.2
ATF27-4	198	186	0.97	232.9[a]	2.8	26.81	1.2	0.0619	3.4
ATF27-6	3790	4102	1.12	178.2[a]	4.6	17.71	0.8	0.4516	1.9
ATF31-7	452	176	0.40	416.5	3.8	14.98	0.9	0.0553	1.6
ATF31-5	260	60	0.24	416.0	4.2	14.99	1.0	0.0560	2.1
ATF31-3	296	91	0.32	409.1	5.6	15.20	1.4	0.0579	1.9
ATF31-1	706	301	0.44	408.4	3.9	15.24	1.0	0.0573	1.3
ATF31-4	156	52	0.34	403.2	4.6	15.44	1.2	0.0577	2.6
ATF31-6	363	144	0.41	401.8	3.8	15.45	0.9	0.0600	1.7
ATF31-8	1893	30	0.02	248.3	2.0	25.26	0.8	0.0578	1.3
ATF31-9	2417	70	0.03	242.4	2.3	25.12	0.9	0.0811	4.3
ATF31-2	324	113	0.36	393.6[b]	3.8	15.85	1.0	0.0563	1.9
ATF31-10	278	85	0.32	367.9[c]	4.0	16.98	1.1	0.0564	4.0
ATF31-11	2701	119	0.05	205.0[a]	1.7	27.96	0.8	0.1275	1.5
ATF-X2-3	186	103	0.57	259.4	3.1	24.32	1.2	0.0526	3.2
ATF-X2-2	1475	402	0.28	254.6	2.1	24.82	0.8	0.0512	1.2
ATF-X2-7	807	352	0.45	253.9	2.2	24.83	0.9	0.0535	1.5
ATF-X2-6	1221	306	0.26	251.1	2.1	25.11	0.8	0.0535	1.2
ATF-X2-4	630	383	0.63	250.2	2.4	25.29	1.0	0.0506	1.8
ATF-X2-5	1712	667	0.40	249.9	2.0	25.31	0.8	0.0510	1.1
ATF-X2-1	387	165	0.44	247.5	2.5	25.48	1.0	0.0535	2.2

[a] Samples with lead loss.
[b] Inheritance zircon ages.
[c] Mixed ages between rim and core.

4. Concluding remarks

In summary, the magmatic and metamorphic history deduced from the SHRIMP zircon dating results indicates that the granitic clasts in the upper Lower Miocene and the overlying Miocene strata were derived from the southern Qilian Shan and northern Qaidam regions. The distance between the depositional site in the Xorkol basin and the most distant late Paleozoic granite across the fault defines the maximum possible post-Early Miocene slip as 165 km. Assuming the Early/Mid-

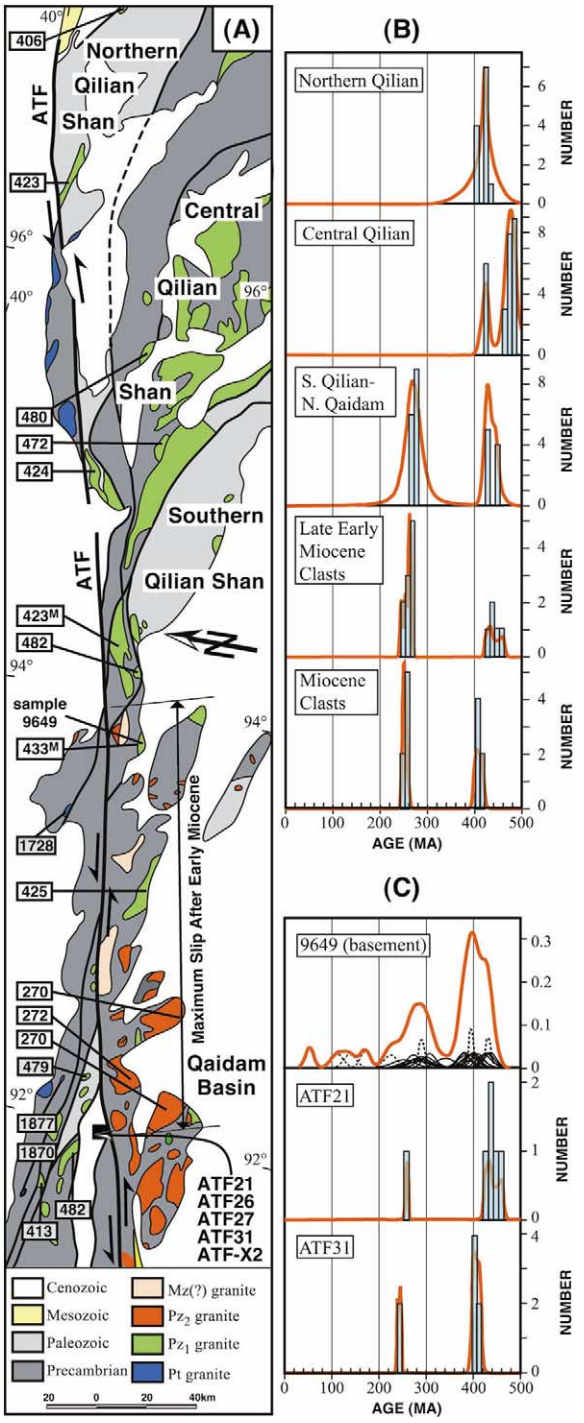

dle Miocene boundary to be 16.4 Ma [34], an upper bound on the post-Early Miocene long-term slip rate is 10 mm/year.

Placing an upper bound on the long-term slip rate of the ATF is important for resolving some important problems of Asian tectonics. First, this upper bound illustrates that the ATF has predominantly been a low-slip-rate fault since the Early/Middle Miocene boundary. This result is consistent with low Quaternary slip-rate estimates [9,10] and low present-day slip-rate measurements [7,8], and suggests that these low slip-rate estimates are applicable as early as the Middle Miocene. Hence, our result supports the idea that distributed shortening, not lateral extrusion, has been the dominant deformation mechanism since the Middle Miocene [4–6]. This upper bound is not compatible with higher Quaternary slip-rate estimates of 20–30 mm/year [19–22] unless a dramatic slip-rate increase happened in the late Quaternary. Alternatively, recent suggestions that some of the high slip-rate estimates (e.g. [20]) are due to underestimation of the ages of offset features, may resolve this apparent discrepancy with Quaternary–Recent slip rates [35].

Second, the low upper bound on the long-term slip rate along the ATF implies a low long-term slip rate along the Haiyuan fault (Fig. 1), whose offset is considered to be transferred from the ATF [36]. This supports the previous low slip-rate estimates ($\sim$5 mm/year [37]; 7.5 ± 2.5 mm/year [38]) on the Haiyuan fault and suggests that this fault is not an important extrusion boundary.

Third, recently documented evidence for large cumulative offset of pre-earliest Miocene features along the ATF [11–18] and the evidence for a low post-Early Miocene long-term slip rate presented

←

Fig. 7. Correlation between the SHRIMP zircon dating results of the Miocene clasts in the Xorkol basin and the basement to the south of the ATF. (A) Ages of granitoids in Qilian Shan and Qaidam. (B) Crystallization–age correlation. (C) Metamorphic–history correlation. Radiometric dating method for basement is single-grain zircon U–Pb, except for those with superscript M, which means monazite U–Th–Pb [32,33]. Ages in white boxes are from south of the fault; ages in gray boxes are from north of the fault. Abbreviations used in A: Pt, Proterozoic; Pz_1, early Paleozoic; Pz_2, late Paleozoic; Mz, Mesozoic.

here suggest a substantial amount (>210 km) of late Oligocene–early Miocene slip (Fig. 2). This requires a mid-Tertiary slip rate of 17 mm/year or higher, and suggests that the ATF may have accommodated extrusion before the late Early Miocene. It should be noted that the new slip curve (solid line in Fig. 2) represents a conservative estimate for the late Oligocene–Early Miocene slip rate, which could be even higher. This change from late Oligocene–Early Miocene fast slip and extrusion to Early Miocene–present slow slip and crustal thickening supports a two-stage evolution [23], which reconciles the two conflicting mechanical hypotheses, and provides a mechanism for the mid-Miocene exhumation of northern Tibet [39]. The dominance of young crustal thickening explains why geodetic measurements of slip rates and magnitude of offset on faults (e.g. Red River fault) in the eastern Tibetan Plateau are too low to support lateral extrusion [40]. In addition, the two-stage model explains why the ATF cannot be traced northeast of the Qilian Shan as a geomorphic feature, although it probably extended beyond that mountain range before the mid-Miocene [23]; instead, the currently active ATF ends at the Qilian Shan, where strike-slip is accommodated by shortening.

Acknowledgements

We thank P. Molnar and R. Ingersoll for critical and constructive reviews and J.G. Liou and M. McWilliams for helpful discussions. This work was supported by two Stanford McGee grants, a GSA Graduate Student grant and an AAPG Grant-in-Aid to Y.Y., and US National Science Foundation grants to S.A.G. (EAR-0207364), B.D.R. (EAR-0207115), and G.E.G. (EAR-9725663).*[BOYLE]*

References

[1] X. Le Pichon, M. Fournier, L. Jolivet, Kinematics, topography, shortening, Tectonics 11 (1992) 1085–1098.
[2] P. Tapponnier, G. Peltzer, A.Y. Le Dain, R. Armijo, P. Cobbold, Propagating extrusion tectonics in Asia; new insights from simple experiments with plasticine, Geology 10 (1982) 611–616.
[3] P. Tapponnier, Z. Xu, F. Roger, B. Meyer, N. Arnaud, G. Wittlinger, J. Yang, Oblique stepwise rise and growth of the Tibet Plateau, Science 293 (2001) 1671–1677.
[4] P.C. England, G.A. Houseman, Finite strain calculations of continental deformation, 2, Comparison with the India-Asia collision zone, J. Geophys. Res. 91 (1986) 3664–3676.
[5] J.F. Dewey, S. Cande, W.C. Pitman, Tectonic evolution of the India/Eurasia collision zone, Eclogae Geol. Helv. 82 (1989) 717–734.
[6] P.C. England, P. Molnar, Active deformation of Asia: from kinematics to dynamics, Science 278 (1997) 647–650.
[7] R. Bendick, R. Bilham, J. Freymueller, K. Larson, G. Yin, Geodetic evidence for a low-slip rate in the Altyn Tagh fault system, Nature 404 (2000) 69–72.
[8] Z. Shen, M. Wang, Y. Li, D.D. Jackson, A. Yin, D. Dong, P. Fang, Crustal deformation along the Altyn Tagh Fault system, western China, from GPS, J. Geophys. Res. 106 (2001) 30607–30621.
[9] Altyn Tagh Fault Seismic Zone Group of State Seismic Bureau, Altyn Tagh Fault Zone, Seismic Publishing House, Beijing, 1992, 319 pp.
[10] Z. Washburn, J.R. Arrowsmith, S.L. Forman, E. Cowgill, X. Wang, Y. Zhang, Z. Chen, Late Holocene earthquake history of the central Altyn Tagh fault, China, Geology 29 (2001) 1051–1054.
[11] J. Cui, Z. Tang, J. Deng, Y. Yue, Q. Yu, L. Meng, The Altyn Tagh Fault System, Geological Publishing House, Beijing, 1999, 249 pp.
[12] B.D. Ritts, U. Biffi, Magnitude of post-Middle Jurassic (Bajocian) displacement on the Altyn Tagh fault, NW China, Geol. Soc. Am. Bull. 112 (2000) 61–74.
[13] E.R. Sobel, N. Arnaud, M. Jovilet, B.D. Ritts, M. Brunel, Jurassic exhumation history of the Altyn Tagh range, NW China, Geol. Soc. Am. Mem. 194 (2001) 247–267.
[14] J. Yang, Z. Xu, J. Zhang, C. Chu, R. Zhang, J.G. Liou, Tectonic significance of Caledonian high-pressure rocks in the Qilian-Qaidam-Altun mountains, NW China, Geol. Soc. Am. Mem. 194 (2001) 151–170.
[15] Y. Yue, J.G. Liou, S.A. Graham, Tectonic correlation of Beishan and Inner Mongolia orogens and its implications for the palinspastic reconstruction of north China, Geol. Soc. Am. Mem. 194 (2001) 101–116.
[16] J. Zhang, Z. Zhang, Z. Xu, J. Yang, J. Cui, Petrology and geochronology of eclogites from the western segment of the Altyn Tagh, northwestern China, Lithos 56 (2001) 187–206.
[17] Y. Yue, B.D. Ritts, S.A. Graham, Initiation and long-term slip history of the Altyn Tagh fault, Int. Geol. Rev. 43 (2001) 1087–1093.
[18] G.E. Gehrels, A. Yin, X. Wang, Detrital-zircon geochronology of the northeastern Tibet Plateau, Geol. Soc. Am. Bull. 115 (2003) 881–896.
[19] P.J. Aouac, P. Tapponnier, Kinematic model of active

deformation in central Asia, Geophys. Res. Lett. 20 (1993) 895–898.
[20] G. Peltzer, P. Tapponnier, R. Amijo, Magnitude of the Quaternary left-lateral displacements along the north edge of Tibet, Science 246 (1989) 1285–1289.
[21] A.S. Meriaux, F.J. Ryerson, P. Tapponnier, J. Van de Woerd, R. Finkel, Fast extrusion of the Tibet Plateau: A 3 cm/yr, 100 kyr slip rate on the Altyn Tagh fault, EOS 81 (2000) 1137.
[22] F.J. Ryerson, G. Peltzer, P. Tapponnier, R. Finkel, A.S. Meraux, J. Van de Woerd, M.W. Caffee, Active slip-rates on the Altyn Tagh fault Karakax valley segement: constraints from surface exposure dating, EOS 80 (1999) 1008.
[23] Y. Yue, J.G. Liou, A two-stage evolution model for the Altyn Tagh fault, China, Geology 27 (1999) 227–230.
[24] Y. Yue, Slip History of the Altyn Tagh Fault and Its Implications for Tectonics of Asia, Ph.D. Thesis, Stanford University, Stanford, CA, 2003.
[25] Z. Che, L. Liu, H. Liu, J. Luo, Discovery and occurrence of high-pressure metapelitic rocks from Altun Mountain areas, Xinjiang Autonomous Region, Chin. Sci. Bull. 40 (1995) 1988–1991.
[26] Xinjiang Bureau of Geology and Mineral Resources, 1:200,000 Regional Geological Investigation Report (J-46-VIII), 543 Publishing Factory, Xi'an, 1982, 224 pp.
[27] Qinghai Bureau of Geology and Mineral Resources, Regional Geology of Qinghai Province, Geological Publishing House, Beijing, 1991, 662 pp.
[28] F. Yang, W. Tang, J. Wei, Z. Fu, S. Liang, Tertiary in Petroliferous Regions of China, Volume II: The Northwestern Region of China, Oil Industrial Publishing House, Beijing, 1994, 253 pp.
[29] B.D. Ritts, Y. Yue, S.A. Graham, Oligocene–Miocene tectonics and sedimentation along the Altyn Tagh fault, northern Tibetan Plateau: Analysis of the Xorkol, Subei, and Aksay basins, J. Geol. 112 (2003) in press.
[30] D. Gebauer, H.P. Schertl, M. Brix, W. Schreyer, 35 Ma old ultrahigh-pressure metamorphism and evidence for very rapid exhumation in the Dora Maira Massif, Western Alps, Lithos 41 (1997) 5–24.
[31] Gansu Bureau of Geology and Mineral Resources, Regional Geology of Gansu Province, Geological Publishing House, Beijing, 1989, 692 pp.
[32] N. Delville, N. Arnaud, J.-M. Montel, F. Roger, M. Brunel, P. Tapponnier, E. Sobel, Paleozoic to Cenozoic deformation along the Altyn Tagh Fault in the Altun Shan Massif area, eastern Qilian Shan, northeastern Tibet, China, Geol. Soc. Am. Mem. 194 (2001) 269–292.
[33] G. Gehrels, A. Yin, X. Wang, Magmatic history of the northeastern Tibet Plateau, J. Geophys. Res. 108 (2003) doi: 10.1029/2002JB001876.
[34] A.R. Palmer, J. Geissman, 1999. Geological Time Scale, Geological Society of America, Boulder, CO, 1999.
[35] R. Heztel, S. Niedermann, M. Tao, P.W. Kubik, S. Ivy-Ochs, B. Gao, M. Strecker, Low slip rates and long-tern preservation of geomorphic features in Central Asia, Nature 417 (2002) 428–432.
[36] B. Meyer, P. Tapponnier, L. Bourjot, F. Metivier, Y. Gaudemer, G. Peltzer, S. Guo, Z. Chen, Crustal thickening in Gansu-Qinghai, lithospheric mantle subduction, and oblique, strike-slip controlled growth of the Tibet platea, Geophys. J. Int. 135 (1998) 1–47.
[37] B. Liu, J. Zhou, The research on the active Haiyuan fault in China, Northwest Seismol. J. 8 (1986) 79–88.
[38] B.C. Burchfiel, P. Zhang, Y. Wang, W. Zhang, F. Song, Q. Deng, P. Molnar, L. Royden, Geology of the Haiyuan fault zone, Ningxia-Hui Autonomous Region, China, and its relation to the evolution of the northeastern margin of the Tibetan Plateau, Tectonics 10 (1991) 1091–1110.
[39] A.D. George, S.J. Marshallsea, K.-H. Wyrwoll, J. Chen, Y. Lu, Miocene cooling in the northern Qilian Shan, northeastern margin of the Tibetan Plateau, revealed by apatite fission-track and vitrinite-reflectance analysis, Geology 29 (2001) 939–942.
[40] B.C. Burchfiel, R. King, L.H. Royden, E. Wang, Z. Chen, Y. Liu, W. Tang, J. Zhao, Y. Zhang, The late Cenozoic evolution of the eastern part of the Tibetan Plateau, Geol. Soc. Am. Abstr. Programs 31 (1999) 66.
[41] E. Wang, Displacement and timing along the northern strand of the Altyn Tagh fault zone, northern Tibet, Earth Planet. Sci. Lett. 150 (1997) 55–64.
[42] A. Yin, G. Gehrels, X. Chen, X. Wang, Evidence for 280 km of Cenozoic left slip motion along the eastern segment of the Altyn Tagh fault, EOS Trans. Am. Geophys. Union 80 (1999) 1018.